In-flight structural identification:input/output versus output-only data processing

Laurent Mevel, Albert Benveniste, Michèle Basseville, Maurice Goursat, Bart Peeters, Herman van Der Auweraer, Antonio Vecchio

INRIA

INSTITUT NATIONAL DE RECHERCHE EN INFORMATIQUE ET EN AUTOMATIQUE

In-flight structural identification: input/output versus output-only data processing

Laurent Mevel, Albert Benveniste, Michèle Basseville, Maurice Goursat

Bart Peeters, Herman Van der Auweraer, Antonio Vecchio

N°5108

February 2004

THÈME 4

ISSN 0249-6399 ISRN INRIA/RR--5108--FR+ENG

In-flight structural identification: input/output versus output-only data processing

Laurent Mevel, Albert Benveniste, Michèle Basseville*, Maurice Goursat†,
Bart Peeters, Herman Van der Auweraer, Antonio Vecchio‡

Thème 4 — Simulation et optimisation
de systèmes complexes
Projets Sigma2 et Metalau

Rapport de recherche n ° 5108 — February 2004 — 34 pages

Abstract: The problem of in-flight data analysis, for the purpose of structural model identification under *both* measured and uncontrolled non-stationary excitation, is addressed. Input/output and output-only eigenstructure identification methods are described and compared, within two classes of methods: subspace-based and prediction error. In particular, different types of relevant projections for handling the known (measured) and unknown (uncontrolled) inputs are discussed. The relevance of the methods is emphasized through numerical results obtained on flight test data sets.

Key-words: In-operation structural analysis, subspace-based eigenstructure identification, prediction error identification, input/output versus output-only identification, in-flight data analysis, flutter monitoring.

(Résumé : tsvp)

This work has been carried out within the framework of the Eurêka project no 2419 FLITE (**Fli**ght **T**est **E**asy), coordinated by Sopemea, Velizy-Villacoublay, France.

* IRISA – Laurent.Mevel,Albert.Benveniste,Michele.Basseville@irisa.fr.
L.M. and A.B. are with INRIA, M.B. is with CNRS.
† INRIA Rocquencourt, Projet Metalau – Maurice.Goursat@inria.fr.
‡ LMS International, Researchpark Haasrode Z1, Interleuvenlaan 68, 3001 Leuven, Belgium – Bart.Peeters,Herman.VanderAuweraer,Antonio.Vecchio@lms.be.

Unité de recherche INRIA Rennes
IRISA, Campus universitaire de Beaulieu, 35042 RENNES Cedex (France)
Téléphone : 02 99 84 71 00 - International : +33 2 99 84 71 00
Télécopie : 02 99 84 71 71 - International : +33 2 99 84 71 71

Identification de structures en vol: traitement de données entrées/sorties versus sorties seules

Résumé : On étudie le problème du traitement des données de vols d'avions, dans le but d'identifier le comportement dynamique de la structure dans les deux situations où les excitations sont mesurées ou/et non contrôlées. On décrit et compare des méthodes d'identification de structure propre, travaillant avec des mesures entrées/sorties ou/et sorties seules, et relevant de deux classes distinctes: les méthodes par sous-espaces, et les méthodes basées sur l'erreur de prédiction. On discute en particulier différents types de projections adaptées à la prise en compte des entrées connues (mesurées) et des entrées inconnues (non contrôlées). La pertinence des méthodes est illustrée par des résultats numériques obtenus sur des données réelles de vols.

Mots-clé : Analyse structurale en fonctionnement, identification de structure propre par sous-espaces, identification basée sur l'erreur de prédiction, identification entrées/sorties versus sorties seules, analyse de données de vols d'essais, surveillance du phénomène dit de flutter.

1 Introduction

Both practical and conceptual motivations are provided for the input/output and output-only structural identification methods discussed in the paper.

Practical motivations. Experimental Modal Analysis (EMA) is currently one of the key technologies in structural dynamics analysis. Based on the academic foundations of system identification, it has evolved to become a "standard" approach in mechanical product development. Essential in this evolution is that modal analysis research has, from the start, taken the point of view of industrial applicability, focusing on solving the specific problems related to testing and modeling large industrial structures (see also section 4.4). The merit of each new method or new approach has always been checked against the added value it brought in terms of helping the application engineers to derive better models.

A nice example is the development cycle of a new aircraft, which consists of several modeling and testing stages: structural finite element (FE) modeling, ground vibration testing (GVT), computational fluid dynamics (CFD) modeling, wind tunnel testing, and in-flight tests. These flight (vibration) tests allow the validation of the analytical models under various real flight conditions and, more important, allow to assess the aero-elastic interaction, as a function of airspeed and altitude, between the structure and the aerodynamic forces as they may lead to a sudden unstable behavior known as flutter. Flutter shows up in the vibration signals as apparent negative damping and corresponding sudden increase of the vibration amplitudes. For economic and safety reasons (i.e. to avoid a loss of the aircraft), it is evidently avoided that an aircraft goes into flutter during an in-flight test, but it has to be certified that it has sufficient flutter margin when flying at the different points of the flight envelope where it is designed for. To determine this margin, typically, the trends of eigenfrequencies and damping ratios of the critical modes as a function of airspeed are carefully studied [24, 37]. This explains the need to perform system identification during the flight.

Current practice is to apply and measure artificial excitation (the inputs) during the flight and measure the aircraft acceleration response at various locations (the outputs). Various solutions were developed to provide this dynamic excitation during the flight such as excitation through the control surfaces or wing-tip excitation by aerodynamic vanes [24]. A recent trend in flight-testing is the use of atmospheric turbulences as excitation sources. The greatest attraction to this type of excitation is that no special on-board exciter hardware is required. Then the typical situation

is that it is practically impossible to measure the forces acting on the aircraft and that the deterministic knowledge of the input is replaced by the assumption that the input is white noise.

Conceptual motivations. It is known [16, 22, 35, 6] that the modes and mode-shapes of a mechanical structure coincide with the eigenstructure of a continuous time MIMO linear system driven by an excitation, and whose output vector is the set of accelerometer measurements. Because of what has been argued above, the key issue is to identify the eigenstructure in the presence of *both* a natural (unknown, unmeasured and non-stationary) excitation and a controlled (known, measured) input. This setup is frequently referred to as *input/output* [15].

Handling both controlled inputs and unknown excitations should take advantage of the available knowledge on the controlled inputs, and thus should rely on input/output identification methods. However, it is of interest to understand that involving the input data can be done with *minor* modification of output-only identification methods to be used for eigenstructure identification in-operation, that is in the presence of natural excitation [35, 7].

During the last decade, there has been a growing interest in and investigation of subspace-based linear system identification methods [34, 45, 44, 43] and their relationship with instrumental variables [46]. These methods are well suited for capturing the system eigenstructure, even without observed inputs [9]. On the other hand, the recent polyreference LSCF method [18, 36, 14] is a special implementation of a matrix fraction description (MFD) based usual prediction error method for eigenstructure identification, which can be run under either input-output or output-only form.

The purpose of this paper is to discuss different types of projections which can be performed for handling, separately or simultaneously, the known and unknown inputs within the framework of the covariance driven subspace-based structural identification method; to review the recent polyreference LSCF input-output and output-only eigenstructure identification methods and re-cast them in a framework closely related to the subspace methods; and to investigate the relevance of both classes of methods for in-flight data analysis by reporting on numerical results obtained on real data sets.

Paper outline. In section 2, the key elements of *subspace-based covariance-driven* eigenstructure identification are recalled, and how to process *time-domain* input/output data and to handle both known and unknown inputs, is explained. In section 3, the

key elements of a recent *matrix fraction description*-based implementation of the prediction error methods are introduced under both input-output and output-only forms, and related to the subspace-based methods. In section 4, numerical results obtained on real data sets are reported, and the two types of methods and input handling are discussed. Section 5 contains further comments and conclusions.

2 Subspace-based eigenstructure identification

The use of state-space representations for modal analysis is well known [16, 22, 35, 6]. It has been recognized that the eigenstructure of the state transition matrix F of a discrete time linear model is in one-to-one correspondence with the structural modes (eigenvalues) and mode-shapes (eigenvectors); see the Appendix for further details. The use of either covariance-driven or data-driven subspace-based identification algorithms for structural analysis has thus been advocated [39, 1, 35, 7]. The use of the covariance-driven algorithm might be appealing when processing long samples of multi-sensor output measurements, which can be mandatory for in-operation structural analysis under non-stationary environment. In this section, we describe covariance-driven subspace-based identification algorithms for the combined handling of known and unknown inputs.

2.1 Fundamentals of covariance-driven identification algorithms

Throughout the paper, we perform a repeated use of the following elementary remark, which belongs to the folklore of system or matrix theory. Consider a pair (H, F) of matrices, respectively $r \times n$ and $n \times n$. Let $R \stackrel{\Delta}{=} (R_i)_{i \geq 0}$ be a sequence of matrices such that R_i decomposes as :

$$R_i = HF^{i-1}G \tag{1}$$

for some matrix G, independent from i. Then the (infinite) Hankel matrix :

$$\mathcal{H}(R) \stackrel{\Delta}{=} \begin{bmatrix} R_1 & R_2 & R_3 & R_4 & \dots \\ R_2 & R_3 & R_4 & R_5 & \dots \\ R_3 & R_4 & R_5 & R_6 & \dots \\ \dots & \dots & \dots & \dots & \dots \end{bmatrix} \tag{2}$$

factors out as : $\mathcal{H}(R) = \mathcal{O}(H,F)\ \mathcal{C}(F,G)$, where : $\mathcal{O}(H,F) \stackrel{\Delta}{=} \begin{bmatrix} H \\ HF \\ HF^2 \\ \vdots \end{bmatrix}$ and $\mathcal{C}(F,G) \stackrel{\Delta}{=} [\ G \quad FG \quad F^2G \quad \dots\ ]$. Such a factorization is unique up to a post-

multiplication of $\mathcal{O}(H,F)$ by an invertible matrix. Then, up to a change of basis on F, the pair (H,F) can be recovered from the first block-row and the shift invariant property of $\mathcal{O}(H,F)$, respectively. The eigenstructure is then extracted from F. See the Appendix for the definitions and subsection 4.1 for the implementation details.

All this is routine and is only recalled to point out that, throughout this section, we consider that *we get a new algorithm each time we are handling another factorization of the form (1).*

2.2 Handling time domain input/output data

We consider a linear time-invariant state space system with a *combined* controlled input excitation U_k and ambient excitation V_k :

$$\left\{ \begin{array}{rcll} X_k & = & F\ X_{k-1} + D\ U_k + V_k\ , & \mathbf{cov}(V_k) = Q_V \\ Y_k & = & H\ X_{k-1} + v_k\ , & \mathbf{cov}(v_k) = Q_v \end{array} \right. \tag{3}$$

where the inputs (U_k) and (V_k) and the measurement noise (v_k) are unmeasured zero mean Gaussian white noise sequences. We stress that sinusoidal or colored input excitation (V_k) can be encompassed as well [39, 7]. Note that the measurement noise (v_k) does not affect the eigenstructure of (3), and that a moving average sequence (v_k) can also be encompassed [43, 6]. The different signals, and in particular the inputs (U_k), are assumed to be stationary. Arguments similar to those in [12, 31] can be used for relaxing this assumption; this will be addressed elsewhere. Furthermore, we assume that :

Measurement noise v_k is uncorrelated from both inputs U_k and V_k; (4)

Observed and unobserved inputs are uncorrelated; (5)

Observed and unobserved inputs are both white. (6)

Condition (6) may seem questionable regarding the *observed* input U_k. However, it can be enforced possibly after a proper whitening.

For recovering the eigenstructure of (3), our approach consists in handling different projections of the system onto the subspace generated by all the observed inputs, or onto its orthogonal subspace. Formally, the set of zero mean finite covariance random variables is equipped with the scalar product : $\langle x,y\rangle \stackrel{\Delta}{=} \mathbf{E}(xy)$. Then, if $\mathcal{U}$ denotes the linear space generated by all the inputs :

$$\mathcal{U} = \mathrm{Span}\{U_j : -\infty < j < +\infty\}, \tag{7}$$

its orthogonal is denoted by $\mathcal{U}^\perp$. Now, recovering the eigenstructure of (3) can be performed by using the following projections[1]:

1. Rejecting the unobserved input V by projecting (3) onto $\mathcal{U}$.
2. Rejecting the observed input U by projecting (3) onto $\mathcal{U}^\perp$.
3. Using jointly both projections of (3) onto $\mathcal{U}$ and $\mathcal{U}^\perp$.
4. Mixing the cross- and auto-covariances of the projected outputs.
5. Ignoring the presence of the controlled input U and performing brute force output-only identification.

Using projections in combination with subspace algorithms is not new. It is a very natural idea that is found in several places in the book [43]. However, as the experienced reader will recognize, we exploit this idea under non classical variants. The approaches (1–5) are now described.

Rejecting the unobserved input. Thanks to assumption (5), projecting (3) onto $\mathcal{U}$ amounts to rejecting the unobserved input. This projection writes :

$$\left\{ \begin{array}{rcl} X_k/\mathcal{U} & = & F\ X_{k-1}/\mathcal{U} + D\ U_k \\ Y_k/\mathcal{U} & = & H\ X_{k-1}/\mathcal{U} \end{array} \right. \tag{8}$$

Setting for short $Z^{\mathcal{U}} \triangleq Z/\mathcal{U}$ when there is no risk of confusion, (8) rewrites :

$$\left\{ \begin{array}{rcl} X_k^{\mathcal{U}} & = & F\ X_{k-1}^{\mathcal{U}} + D\ U_k \\ Y_k^{\mathcal{U}} & = & H\ X_{k-1}^{\mathcal{U}} \end{array} \right. \tag{9}$$

For $(W_k)_{k\in Z}$ and $(Z_k)_{k\in Z}$ two zero mean vector random processes, we set :

$$R_i^{WZ} \triangleq \mathbf{E}\left(W_{k+i}\ Z_k^T\right) \tag{10}$$

Using this notation, and thanks to assumption (6), equation (9) gives raise to the following key decompositions of the form (1) :

$$R_i^{Y^{\mathcal{U}}Y^{\mathcal{U}}} = HF^{i-1}G^Y, \text{ where } G^Y \triangleq \mathbf{E}(X_k^{\mathcal{U}}\ Y_k^{\mathcal{U}T}) \tag{11}$$

$$R_i^{Y^{\mathcal{U}}U} = HF^{i-1}G^U, \text{ where } G^U \triangleq \mathbf{E}(X_k^{\mathcal{U}}\ U_k^T) \tag{12}$$

[1] Since (3) is a dynamical system, it is mandatory to project it on shift-invariant subspaces, this is why *all* the observed input variables are considered in $\mathcal{U}$.

The latter cross-covariances are to be handled in a combined manner; this is introduced as algorithm 4 below.

From now on, **algorithm 1** refers to the method in 2.1 applied to the *auto*-covariances in (11).

Rejecting the observed input. Thanks to assumption (5), projecting (3) onto $\mathcal{U}^\perp$ amounts to rejecting the observed input. This projection writes :

$$\left\{ \begin{array}{rcl} X_k/\mathcal{U}^\perp & = & F\ X_{k-1}/\mathcal{U}^\perp + V_k \\ Y_k/\mathcal{U}^\perp & = & H\ X_{k-1}/\mathcal{U}^\perp + v_k \end{array} \right. \tag{13}$$

Thus, setting for short $Z^\perp = Z/\mathcal{U}^\perp$, we get :

$$\left\{ \begin{array}{rcl} X_k^\perp & = & F\ X_{k-1}^\perp + V_k \\ Y_k^\perp & = & H\ X_{k-1}^\perp + v_k \end{array} \right. \tag{14}$$

From (14), the following key decompositions for the covariance matrices holds :

$$R_i^{Y^\perp Y^\perp} \quad = \quad H\ F^{i-1}\ G^{Y^\perp}, \text{ where } G^{Y^\perp} \stackrel{\Delta}{=} \mathbf{E}\left(X_k^\perp\ {Y_k^\perp}^T\right) \tag{15}$$

Note that there are no known inputs to system (13).

From now on, **algorithm 2** refers to the method in 2.1 applied to the *auto*-covariances in (15).

Combining the unobserved and observed input rejections. Rejecting both the observed input U_k and the unobserved input V_k can be achieved by combining the projections of the output Y_k onto both $\mathcal{U}$ and $\mathcal{U}^\perp$. Collect the two equations (9,14) as follows :

$$\left\{ \begin{array}{rcl} \overline{X}_k & = & F\ \overline{X}_{k-1} + \begin{pmatrix} DU_k & V_k \end{pmatrix} \\ \overline{Y}_k & = & H\ \overline{X}_{k-1} + \begin{pmatrix} 0 & v_k \end{pmatrix} \end{array} \right. \tag{16}$$

where $\overline{X}_k \stackrel{\Delta}{=} \begin{pmatrix} X_k^{\mathcal{U}} & X_k^\perp \end{pmatrix}$ and $\overline{Y}_k \stackrel{\Delta}{=} \begin{pmatrix} Y_k^{\mathcal{U}} & Y_k^\perp \end{pmatrix}$. Consider the covariances :

$$\overline{R}_i^Y \quad \stackrel{\Delta}{=} \quad \mathbf{E}\left[Y_{k+i} \begin{pmatrix} {Y_k^{\mathcal{U}}}^T & {Y_k^\perp}^T \end{pmatrix}\right] \tag{17}$$

Note that :

$$\mathbf{E}\left[Y_{k+i}\ U_k^T\right] \quad = \quad \mathbf{E}\left[Y_{k+i}^{\mathcal{U}}\ U_k^T\right] \tag{18}$$

$$\mathbf{E}\left(Y_{k+i}\ {Y_k^\perp}^T\right) \quad = \quad \mathbf{E}\left(Y_{k+i}^\perp\ {Y_k^\perp}^T\right) \tag{19}$$

Thanks to (18,19) and to (11,12), we have:

$$\overline{R}_i^Y \;=\; [\; R_i^{Y^{\mathcal{U}}Y^{\mathcal{U}}} \qquad R_i^{Y^{\perp}Y^{\perp}} \;] \;=\; HF^{i-1}\,[\; G^Y \qquad G^{Y^{\perp}} \;] \tag{20}$$

Method in 2.1 applied to the *combined auto*-covariances in (20) is now called **algorithm 3**.

Mixing the cross- and auto-covariances of the projected outputs. Consider again the system in (16) and, now, the covariances:

$$\overline{R}_i^U \;\triangleq\; \mathbf{E}\left[Y_{k+i}\;(\; U_k^T \qquad Y_k^{\perp T}\;)\right] \tag{21}$$

Again, thanks to (18,19) and to (11,12), we have:

$$\overline{R}_i^U \;=\; [\; R_i^{Y^{\mathcal{U}}U} \qquad R_i^{Y^{\perp}Y^{\perp}} \;] \;=\; HF^{i-1}\,[\; G^U \qquad G^{Y^{\perp}} \;] \tag{22}$$

Algorithm 4 will refer to the method in 2.1 applied to the *combined cross and auto*--covariances (22).

Ignoring the observed input. One obvious way to ignore the presence of the controlled input U_k consists in performing output-only identification. This way is *a priori* a loss of information, which is confirmed *a posteriori* when comparing input/output and output-only structural identification methods, see section 4. Recall that the output-only covariance-driven subspace identification of the eigenstructure is based on the method in 2.1 applied to the measured output covariances $R_i \triangleq \mathbf{E}\, Y_k\, Y_{k-i}^T$, which we refer to as **algorithm 5**.

Discussion. Subspace methods as described here share a lot of similarities with those described in [44, 43]. Subspace methods in their more general form fit into two different categories. Either they try to recover the state matrices (H, F) from the observability matrix, or they try to recover these matrices from a state estimate (for example using a Kalman filter). Our approach obviously fits into the first category, since we are using the left singular vectors of a weighted Hankel matrix. Different choices for the weights [11] can lead to different methods. Thus, the methods described in this paper can be compared with already existing methods like IV-4SID, basic-4SID, and MOESP [10] which is indeed very similar to algorithm 4 above. Also, algorithm 2 is of the same spirit as the projection algorithm for linear deterministic systems proposed in [43][Chap.2]. Since we use different weights and different

data stacking operations, we get different factorizations of the Hankel matrix. Thus, although all these methods lead to the same left factor, they may have different numerical behaviors.

3 Polyreference LSCF or PEM for eigenstructure identification

The recent polyreference LSCF method [18, 36, 14] is a frequency domain method related in part to the basic prediction error method, when both inputs and outputs are available; see [41][Chap.7] for SISO systems, and [27][Appendix 4A,Chap 7.3] for MIMO systems. By frequency domain method, we mean that measurements are directly collected in the Fourier domain, and are processed in the Fourier domain as well. This method is not new in its principle, but we feel it useful to review it and re-cast it in the classical system identification framework. Only an outline of the method is provided here, and the reader is referred to [18, 36, 14] for implementation details.

3.1 The input/output polyreference LSCF method

Throughout this section we assume a N-size input/output data sample Y_k, U_k. We use the following generic notation: for $x_1, \ldots, x_N$ a N-size time domain data sample, the associated DFT is denoted by :

$$\begin{aligned} \phi_N^x(\omega) &\triangleq 1/\sqrt{N} \sum_{k=1}^{N} x_k \, e^{-j\omega k}, \\ \text{where } \omega = \omega_\ell &\triangleq 2\pi\ell/N, \text{ for } \ell = 1, \ldots, N \end{aligned}$$

and we write ϕ^x instead of ϕ_N^x when the length N of the sample is understood.

Denote by $S(\omega)$ the discrete Fourier domain matrix such that :

$$\phi^Y(\omega) = S(\omega) \; \phi^U(\omega),$$

This matrix S is called the FRF matrix. The polyreference LSCF method has two variants. For both variants, $S(\omega_\ell), \ell = 1, \ldots, N$, is considered as the *measured data* record. For system theoretic concepts, the reader is referred to [23].

Left Matrix-Fraction Description (LMFD) system model. In this form, the following system model is assumed:

$$A(e^{-j\omega_\ell})S(\omega_\ell) - B(e^{-j\omega_\ell}) = V(\omega_\ell), \text{ for } \ell = 0, \ldots, N, \tag{23}$$

where $A(z) = A_0 + A_1 z + \ldots + A_p z^p$ and $B(z) = B_0 + B_1 z + \ldots + B_q z^q$ are matrix polynomials, and $V(\omega_\ell), \ell = 0, \ldots, N$ is a white noise matrix of suitable dimensions over the discrete unit circle, with possibly varying covariance operator. This model amounts to approximating the FRF matrix S by the LMFD form $A^{-1}B$. The eigenstructure of system (3) is obtained as follows: the modes are the pairs (μ, ψ_μ) solutions of the following eigenvalue problem:

$$A(\mu)\ \psi_\mu = 0. \tag{24}$$

Right Matrix-Fraction Description (RMFD) system model. In this form, the following system model is assumed:

$$S(\omega_\ell)\ A(e^{-j\omega_\ell}) - B(e^{-j\omega_\ell}) = V(\omega_\ell), \text{ for } \ell = 0, \ldots, N. \tag{25}$$

This model amounts to approximating the FRF matrix S by the RMFD form BA^{-1}. The eigenstructure of the considered system is obtained as follows: the poles μ are solutions of the following eigenvalue problem:

$$A(\mu)\ \varphi_\mu = 0. \tag{26}$$

The modal participation vector φ_μ associated with μ in (26) is different from ψ_μ in (24), which is the desired mode. But ψ_μ can be easily recovered by approximating – in the least squares sense – $S(\omega)$ by a partial fraction expansion having the μ's as its poles. If the poles are simple, then the corresponding residue matrices T_i in :

$$S(\omega) \approx \sum_{i=1}^{n/2} \left(\frac{T_i}{j\omega - \mu_i} + \frac{T_i^*}{j\omega - \mu_i^*} \right) \tag{27}$$

where the superscript * denotes complex conjugate, have rank one. From (27) we get that $T_i = \psi_{\mu_i}\ \varphi_{\mu_i}^T$, which yields the mode-shape ψ_{μ_i} [18].

Discussion.

1. The two models (23,25) are linear in the parameters, with additive noise. Thus they can be identified via classical linear least squares estimates; we refer the reader to [18, 36, 14] for implementation details. The key point is that it is not needed to estimate the B polynomial, since only A is used for estimating the eigenstructure. This remark can be used to reduce the size of the linear equation solving the LS estimation problem. On the other hand, the covariance operators of the noises are design parameters that can reflect the level of measurement noise for the FRF's in the different frequency bands.

   As it is well known [20], the MFD form (both left and right) suffers from non-identifiability problems, since, e.g., $A^{-1}B$ is invariant by pre-multiplication of both A and B by the same arbitrary invertible matrix. But this is of no harm in our case, since the eigenvalue problem (24) is also invariant under the same pre-multiplication. Thus we only need to make sure that we find a maximal row rank MFD representation; uniqueness of A, however, it is not our concern.

2. If we ignore for a while the noise term in equation (23) for LMFD, then we can post-multiply this equation by $U(\omega_\ell)$, and this yields the data based system model $AY - BU = 0$. Reintroducing noise uncertainties gives raise to the popular linear least-squares prediction error method associated to the system model $AY - BU = v$, that can be handled in both frequency or time-domain [27]. However, this reasoning does not work for the RMFD variant, and we do not know how to relate this method to classical ones from the system identification literature in an easy way.

3. Reasons for considering both variants are more practical than theoretical. Let n be the order of the system (state dimension). Assume that there are many more inputs than outputs, i.e., $\dim(Y) \ll \dim(U)$. Then, *the order* of polynomial matrix A will be much larger in the usual LMFD representation than the one in the RMFD representation. This is in favor of choosing the usual LMFD representation, for the following two reasons: *i)* the least squares algorithm associated with (23) will involve larger lags in $Y_k Y_{k-i}^T$, and *ii)* if we want to explore the least squares solutions by assuming different model orders, then increasing by one the order of polynomial A will increase the assumed model order n by a smaller amount (see the discussion in 4.3 on the use of the so-called stabilization diagrams). Of course, the same arguments are in favor of the RMFD representation (23) in the opposite case, namely when the number

of outputs is much larger than the number of inputs. For the considered application of modal analysis with *controlled* excitation, the second situation is the generic one, and therefore the non classical RMFD representation is preferred in practice when a large number of output measurements is used.

For related discussions and additional information on this method, see [18, 14].

3.2 The output-only polyreference LSCF method

Here we assume the model (3) with $D = 0$, i.e., no measured input is available and the unmeasured input is assumed to be white noise. Denote by $S(\omega)$ the discrete Fourier domain matrix whose (i,j) entry equals $\phi^{Y(i)}(\omega) \cdot \left(\phi^{Y(j)}(\omega)\right)^*$, i.e., the measured cross-spectrum between the ith and jth outputs. Again, $S(\omega_\ell), \ell = 1, \ldots, N$ is considered as the *measured data* record.

The output-only polyreference LSCF method relies on the following basic fact from stochastic realization theory for linear systems [13]. Let $R_Y(z)$ be the spectrum of Y, expand it into a Fourier series $R_Y(z) = \sum_{i=-\infty}^{+\infty} R_i z^i$, and set :

$$R_Y^+(z) = R_0/2 \; + \; \sum_{i=1}^{+\infty} R_i \; z^i, \qquad R_Y^-(z) = R_0/2 \; + \; \sum_{i=-\infty}^{-1} R_i \; z^i$$

The following additive decomposition holds: $R = R^+ + R^-$, where R^+ is called the positive half-spectrum of Y and writes :

$$R^+(z) = H(I - z^{-1}F)^{-1}G + J, \;\; \text{where } J = R_0/2 \text{ and } G = \mathbf{E}(X_k \; Y_k^T)$$

Then, approximating R^+ with a LMFD or RMFD representation as in 3.1 yields (estimates of) the poles of system (3). Finally, the corresponding mode-shapes are estimated using again partial fraction expansion (27).

4 Experimental results

We first outline some implementation issues related to the algorithms of sections 2 and 3. Second, we discuss constraints and requirements of the industrial testing practice, which should be kept in mind for the assessment of the practical applicability of the proposed methods. Then, we present numerical results obtained with the algorithms of sections 2 and 3 on real data sets.

4.1 Practical implementation issues - Subspace algorithms

Truncation. Of course, the doubly infinite linear space (7) is not practical. However, if the input excitation has no pure frequency and if matrix F is stable (no root on the unit circle), then (X_k, Y_k) is nearly independent of $U_{k\pm m}$ for m large enough. So $\mathcal{U}$ in (7) can be truncated and replaced, in (8,13,16), by :

$$\mathcal{U}_k = \begin{bmatrix} U_{k-m} \\ \vdots \\ U_k \\ \vdots \\ U_{k+m} \end{bmatrix}, \tag{28}$$

which spans the truncated linear space $\text{Span}\{U_j : k-m \leq j \leq k+m\}$, Then, the following explicit formulas can be used :

$$\begin{array}{rcl} Y_k^{\mathcal{U}} & \approx & Y_k/\mathcal{U}_k, \text{ and} \\ Y_k^{\perp} & \approx & Y_k - Y_k/\mathcal{U}_k, \text{ where} \\ Y_k/\mathcal{U}_k & = & \mathbf{E}(Y_k\, \mathcal{U}_k^T) \left[\mathbf{E}(\mathcal{U}_k\, \mathcal{U}_k^T)\right]^{\dagger} \mathcal{U}_k, \end{array} \tag{29}$$

and superscript † denotes the Moore-Penrose pseudo-inverse. The effect of these approximations can be analyzed with arguments similar to those in [12, 31]; this will be reported elsewhere. The choice of integer parameters in subspace methods is analyzed in [8].

Empirical estimates. In section 2, everything is based on true covariance matrices and on projections which again involve true covariance matrices, see (29). The implementation consists in approximating the true covariances by their corresponding empirical forms. Generically, for a given N-size sample, referring to (10) :

$$R_i^{WZ} \text{ is replaced by } \widehat{R}_i^{WZ} \triangleq 1/(N-i) \sum_{j=1}^{N} W_{j+i}\, Z_j^T \tag{30}$$

Similarly, for any projection, $Z/\mathcal{U}$ is replaced by its empirical counterpart $\widehat{Z}/\mathcal{U}$, which is, by definition, obtained by using empirical covariance estimates.

Moreover, the argument in 2.1 needs to be slightly adjusted to accommodate for the following two practical facts, namely: *i)* because of the empirical covariance estimates, the factorization (1) is only approximate, and *ii)* only a finite amount of R_i's are available. Hence the Hankel matrix (2) is truncated to p block-rows

and q block-columns. Therefore the factorization of Hankel matrix $\mathcal{H}_{p,q}(R)$ is only approximate, which means that :

$$\mathcal{H}_{p,q}(R) = \mathcal{O}_p(H,F)\ \mathcal{C}_q(F,G) + \text{ residual} \tag{31}$$

where $\mathcal{O}_p$ and $\mathcal{C}_q$ are the truncated observability and controllability matrices, respectively. A standard way to obtain such a factorization consists in performing the SVD of an empirical Hankel matrix $\widehat{\mathcal{H}} \triangleq \text{Hank}\left(\widehat{R}_i^{WZ}\right)$, and its truncation at the desired model order. This yields, in the left factor, an estimate $\widehat{\mathcal{O}}$ for the observability matrix $\mathcal{O}$:

$$\widehat{\mathcal{H}} \approx U\ \Delta\ V^T = U \begin{pmatrix} \Delta_1 & 0 \\ 0 & \Delta_0 \end{pmatrix} V^T \tag{32}$$

$$\widehat{\mathcal{O}} = U\ \Delta_1^{1/2}, \quad \widehat{\mathcal{C}} = \Delta_1^{1/2}\ V^T \tag{33}$$

From $\widehat{\mathcal{O}}$, estimates of (H,F) and of the eigenstructure are recovered as sketched in 2.1 and the Appendix, respectively. In the output-only case, this is known under the name of balanced realization (BR) algorithm [4]. This easily extends to the input/output one [19]. Our experience is that selecting $q = p+1$ in (31) is relevant [7].

Weighting matrices. If we compute and truncate the SVD of a *weighted* empirical Hankel matrix $\widehat{\mathcal{H}}_W \triangleq W_1\ \widehat{\mathcal{H}}\ W_2^T$, with W_1 and W_2 two known invertible matrices, then the factors in (33) write: $\widehat{\mathcal{O}} = W_1^{-1}\ U_W\ \Delta_W^{1/2}$ and $\widehat{\mathcal{C}} = \Delta_W^{1/2}\ V_W^T\ (W_2^T)^{-1}$. A classical approach [5, 3, 26, 11] is to normalize the data such that every singular value lies between 0 and 1, and thus represents the cosine of the angle between the subspaces of the future and the past data. This normalization helps avoiding numerical problems by balancing the effects of the main modes and the less energetic ones. In the output-only case, a usual way to proceed is to choose W_1 and W_2 as the inverses of the empirical covariances of the future and past output measurements. In that case, the weighted empirical Hankel matrix $\widehat{\mathcal{H}}_W$ has norm 1. This approach is known as the canonical variate analysis (CVA) and is particularly useful when the order of the process (X_k) is unknown. Adapting this idea to the input-output method in section 2.2 is easy.

4.2 Practical implementation issues - Polyreference LSCF algorithms

The input/output polyreference LSCF algorithm uses empirical transfer function estimates as primary data, whereas its output-only counterpart requires empirical estimates of output spectra or output half spectra. Extensive discussions on how to obtain these empirical estimates are available in literature [30, 17, 38].

4.3 Practical implementation issues - Stabilization diagrams

A typical problem in estimating a parametric model from data is the determination of the model order. For the present eigenstructure identification problem, the dimension n of the matrix F should be estimated. In the subspace algorithms of section 2, this would amount to estimating p in (31) with $q = p+1$. In the polyreference LSCF algorithms of section 3, this would amount to estimating the denominator polynomial order p. Formal procedures estimate models of different orders and compare these models according to a quality criterion such as Akaike's Final Prediction Error or Rissanen's Minimum Description Length criterion [27]. However, practical experience with the application of system identification methods to structural dynamics data learned that it is a good idea to over-specify the model order; to compute the poles from the model; and to eliminate spurious numerical poles afterwards.

The so-called *stabilization diagram* [21, 28] is a very practical tool to achieve this goal. To construct such a stabilization diagram, a repeated analysis of the same data set is performed, each time for a different model order. The pole values from each analysis are combined in one single diagram, with as horizontal axis the pole frequency and as vertical axis the model order. The pole is indicated by a symbol in this diagram. Poles corresponding to the physical system appear at nearly identical frequency locations for every analysis, which is readily visible in the diagram. To point out that the frequency (resp. damping value and eigenvector) of a pole falls within certain bounds of the result obtained at a one-order lower model, specific symbols are used. The spurious numerical poles will not stabilize at all during this process and can be sorted out of the modal parameter data set more easily. Such a stabilization diagram will be shown in the example section.

4.4 Industrial testing requirements

What is important, in view of the practical applicability of the various methods to full-scale problems, is the way they are able to cope with the constraints and requirements of the industrial testing practice. These include:

- The use of large numbers of response transducers: this may range from 8 to 16 responses in a flutter test, 128 or more sensors in a car road test, to a few hundreds in a laboratory vibration test, such as an aircraft ground vibration test.
- The subdivision of a test in "patches" or sensor groups, leading to non-simultaneously measured data.
- Sensitivity to data preprocessing: re-sampling, re-synchronization, band-filtering, etc.
- The non-whiteness of the (unknown) excitation: e.g. there is no guarantee at all that the atmospheric turbulences can be considered as white noise.
- The non-stochastic nature of the excitation: sweeps, or impulses, through aircraft control surfaces, etc.
- The superposition of large levels of harmonic components: e.g. helicopter rotor frequencies, car engine harmonics, turbine shaft or gear speeds, etc.
- Large data sample sizes, often contaminated with large measurement errors.
- Large model sizes.
- Robustness to model inconsistencies: small variations in system behavior during the test or in-between subsequent "patches".
- Robustness to non-stationary excitation.
- The ease of order selection, including the generation of non-physical poles.
- The computational efficiency, especially in view of large data sample sizes, large sensor count, and large model orders.
- The efficiency in estimating damping ratios.
- The capability to generate confidence intervals.

The answers to these questions are essential in the assessment of the practical applicability of the proposed methods. The next subsection contains a discussion of the problem of in-flight data analysis. More industrial examples can be found in the literature [7, 42].

4.5 Real application example

We now report on identification results obtained on real in-flight measurements provided by Avions Marcel Dassault within the Eurêka project FLITE. Successive data sets are available, and thus the evolution of the modal characteristics with the modifications of the aircraft, for example decreasing fuel mass in the tanks, can be tracked. The experiment involves twelve output sensors and one input sensor.

The subspace-based modal analysis algorithms of section 2 has been run using the Scilab Modal toolbox, which contains all these algorithms, among others [32, 33]. The polyreference LSCF modal analysis algorithms of section 3 has been run using the LMS TestLab toolbox [29].

4.5.1 Results with the subspace-based algorithms

We focus on the comparison of the output-only method with some of the input/output methods described in section 2. All methods have been tested with different window sizes, namely 5000, 10000, 15000 and 20000 samples. It turns out that, *for the present example*, most input/output methods suffer from poor results, especially algorithm 1. Because of the poor quality of this method, it is intuitively natural that, *for the present example* again, the combined methods 3 and 4 do not perform as well as expected. These combined methods should be used preferably in experimental situations where the controlled excitation has better excitation properties. That is why we now focus on the merits of the output-only method (algorithm 5) and the best input/output method (algorithm 2).

In the figures 2 to 7, the frequencies are displayed based on a classical stabilization diagram procedure and using the symbols in figure 1; and the alignments of the damping coefficients and of the MAC values are shown.

Input/output vs output-only. Both stabilization diagrams obtained with the same sample size (10000) in the frequency range of interest are displayed in figure 2. It clearly appears that the input/output method yields more stable stabilization diagrams than the output-only approach. This appears still more clearly when zooming in the frequency band, as in figure 3. In addition to estimating the frequencies, we are also interested in good estimates of the damping coefficients and the mode-shapes. This can be evaluated by the quality of the damping alignment and of the MAC alignment. (Note that the latter is meaningful, because we are using enough sensors). This is done for two specific modes in figures 4 and 5. Comparing the

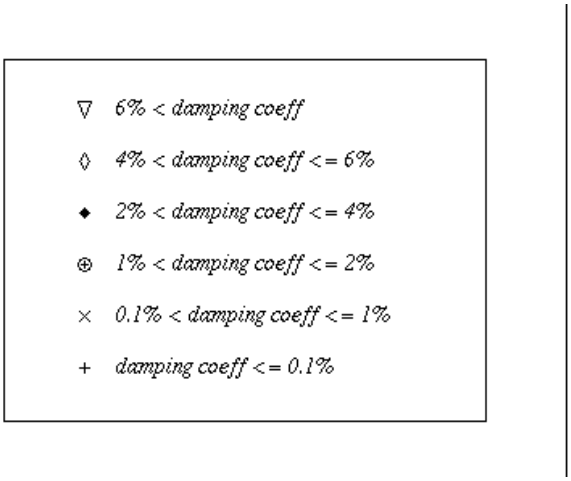

Figure 1: **Subspace** - Meaning of the symbols used in figures 2 to 7.

quality of the stabilization diagrams of each method provides a good information on the superiority of the input/output approach.

Sample size effect. Both methods get better stabilization diagram as the size of the sample used for the identification increases. The input/output results are better than the output-only ones, but the difference in the performances of the input/output and output-only methods decreases when the sample size increases. An example of how the output-only estimates improves when using higher sample sizes is displayed in the damping and MAC diagrams in figure 6. However, it appears that, when processing small records, the input/output method is better than the output-only one.

Merits of using the input. In the results above, we have withdrawn all the input/output approaches, except for method 2, because they gave worse stabilization diagrams, suggesting that the input was not sufficiently exciting within the whole frequency range. Nonetheless, for some modes, it may happen that these methods yield better estimation results. An example of such a situation is displayed in figure 7, where it can be seen that, *for that particular mode*, the combined approaches 3 and 4 give the best (albeit not really good) estimates. For all the other modes, the input/output approaches except for algorithm 2 gave significantly worse results looking at all frequencies, dampings and MACs altogether.

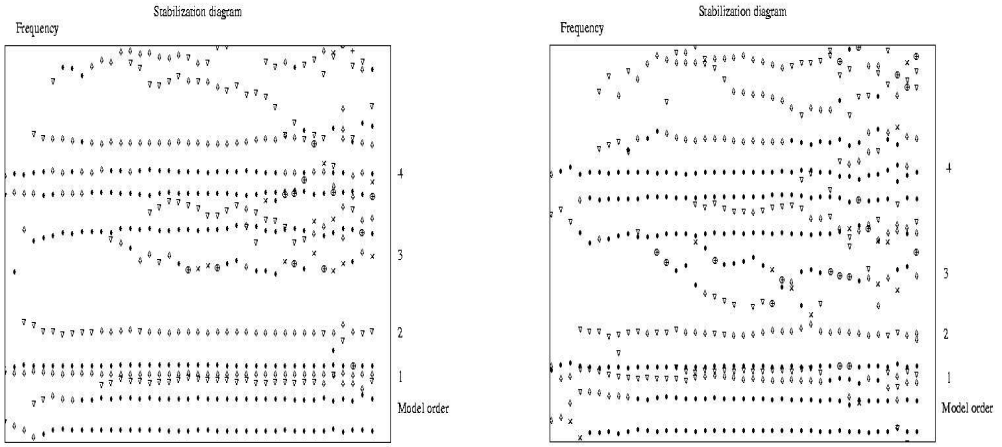

Figure 2: **Subspace** - Frequency stabilization diagram; 4 modes pointed out - Input/output (left), output-only (right).

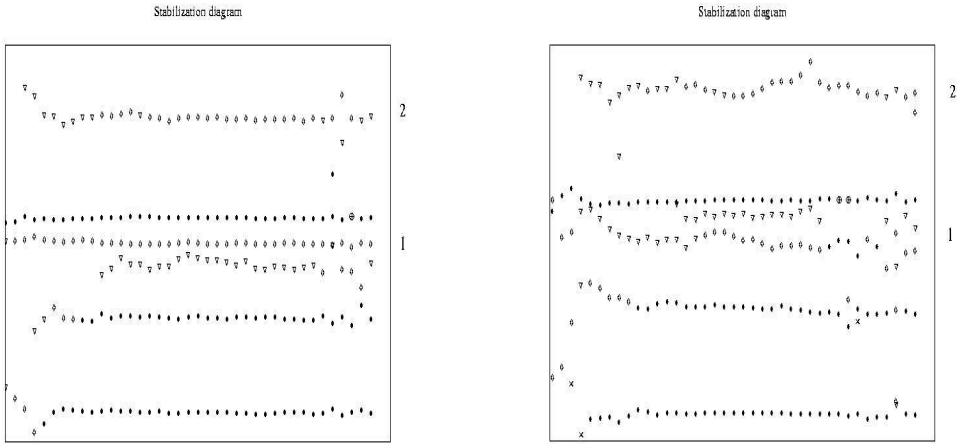

Figure 3: **Subspace** - A closer look at some modes; 2 out of the 4 modes of Fig. 2 pointed out - Input/output (left), output-only (right).

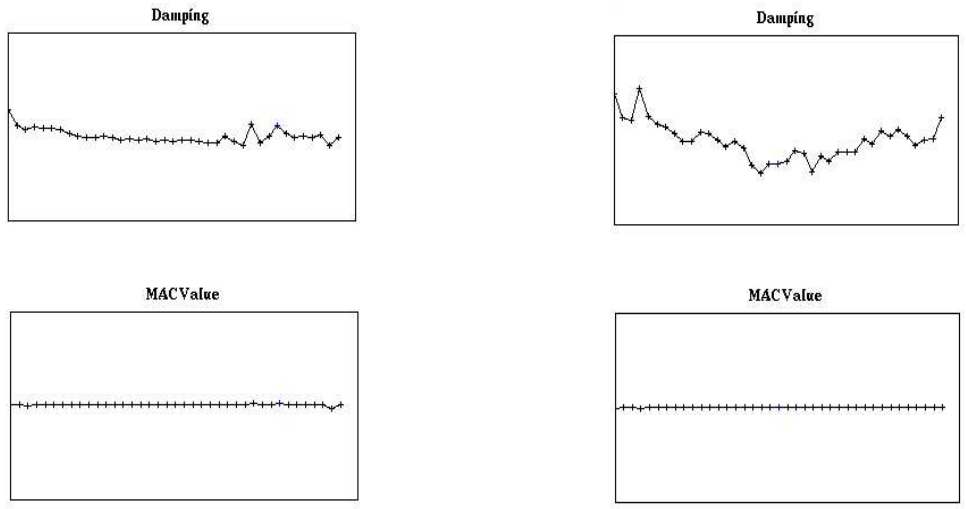

Figure 4: **Subspace** - Damping coefficient (top) and MAC value (bottom) for mode 1 - Input/output (left), output-only (right).

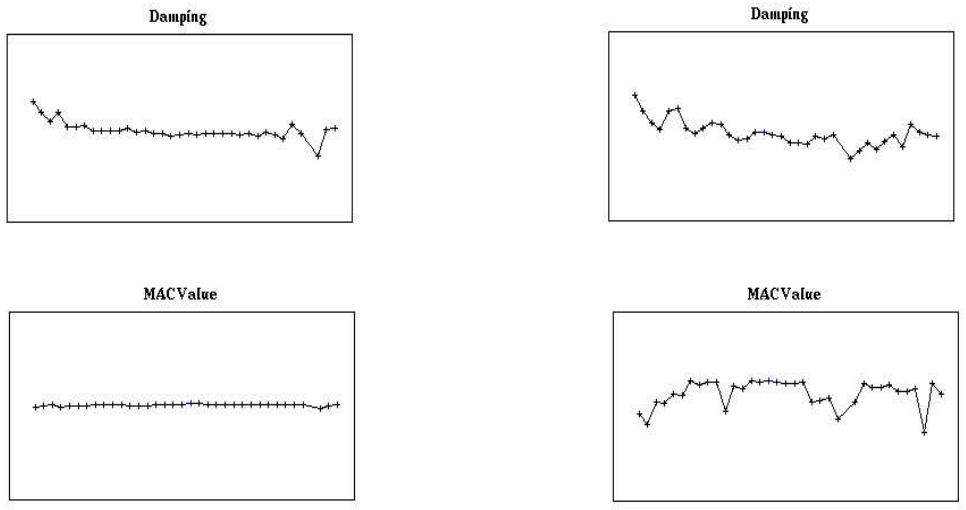

Figure 5: **Subspace** - Damping coefficient (top) and MAC value (bottom) for mode 2 - Input/output (left), output-only (right).

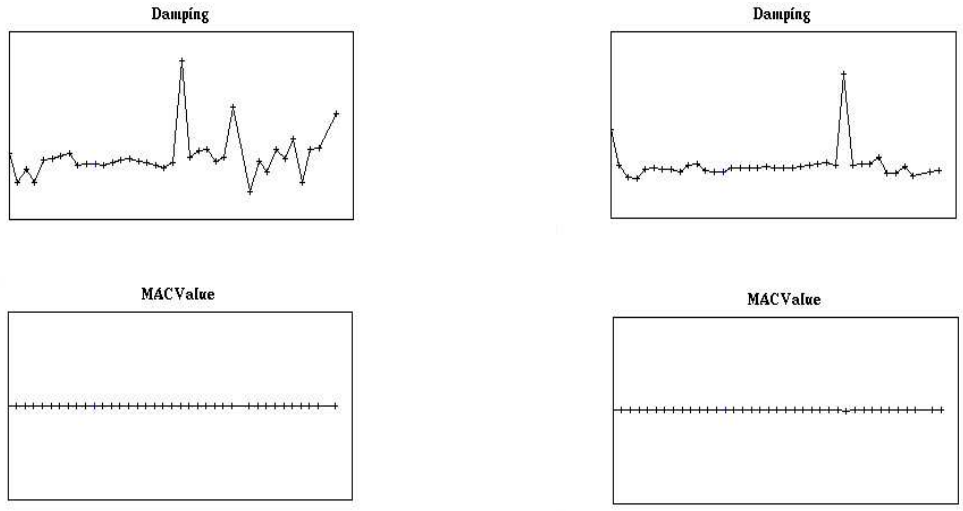

Figure 6: **Subspace** - Window size effect for mode 4: 5000 (left), 10000 (right) - Algorithm 5 (output-only).

This suggests that the input/output subspace methods 1, 3 and 4 in section 2 may have better performance in other applications, when the input signal has better excitation properties, most likely in strictly controlled experiments as in laboratory setups.

4.5.2 Results with the polyreference LSCF algorithms

Both the input/output as the output-only versions of the polyreference LSCF method have been applied to data records of different lengths: 10000, 15000, 20000 samples. In the output-only case, the cross spectra between the outputs and two selected reference outputs served as primary data. In the input/output case, only one input was present and the FRFs between this input and all outputs served as primary data. In order to obtain models with the same number of modes, the maximum denominator polynomial order in the input/output case was chosen to be twice the order in the case of the output-only data.

Input/output vs. output-only. The differences in the stabilization diagrams are rather small, as can be seen on Figure 8. There seems to be more stable poles when using the input information. When looking at the frequency and damping evolution

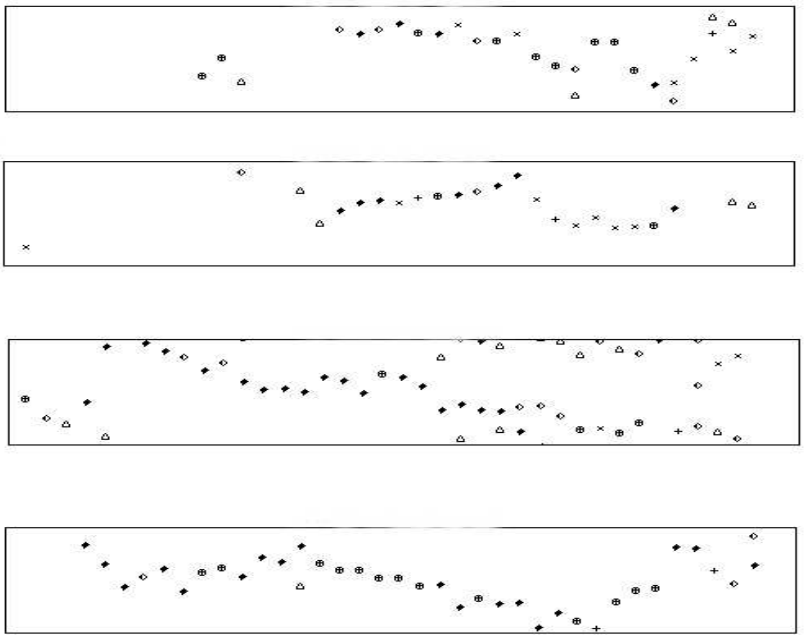

Figure 7: **Subspace** - Input effect on mode 3 - From top to bottom: algorithms 5, 2, 3, 4.

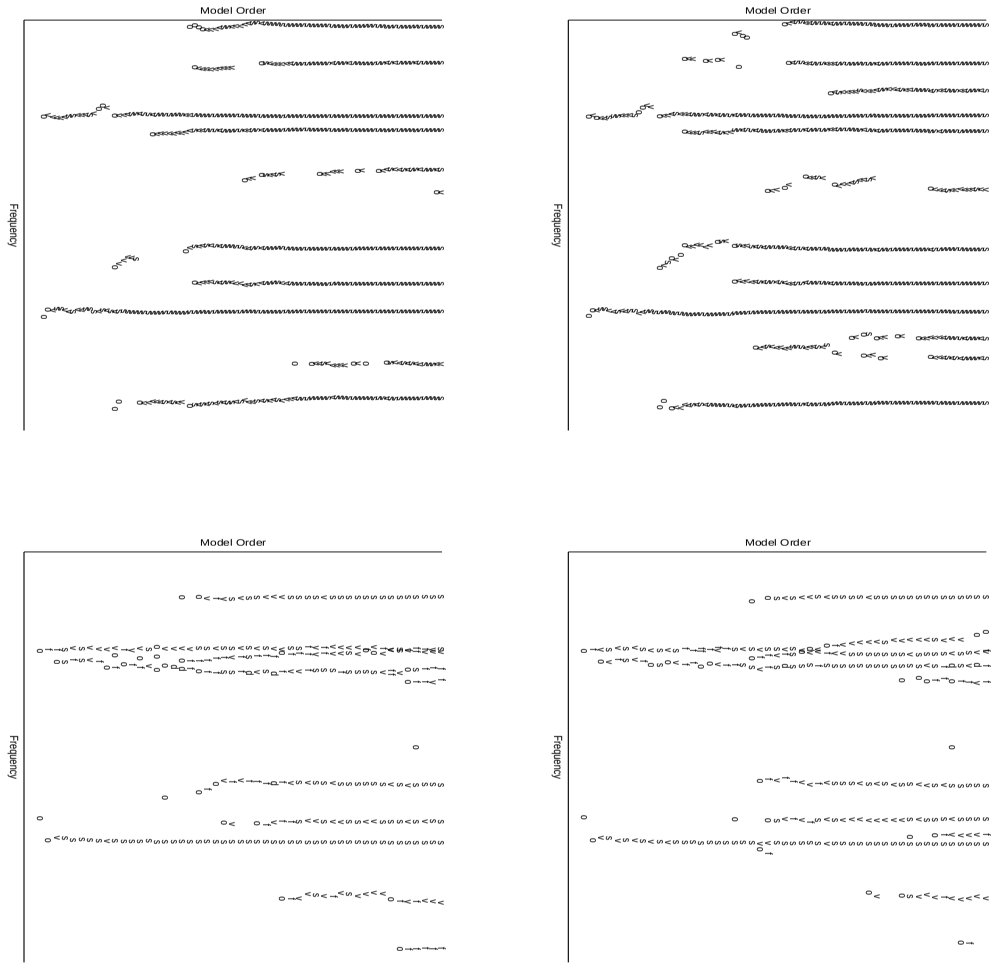

Figure 8: **LSCF** - Stabilization diagram for 10000 samples (Left) and 20000 samples (Right); for input/output (Top) and output-only data (Bottom).

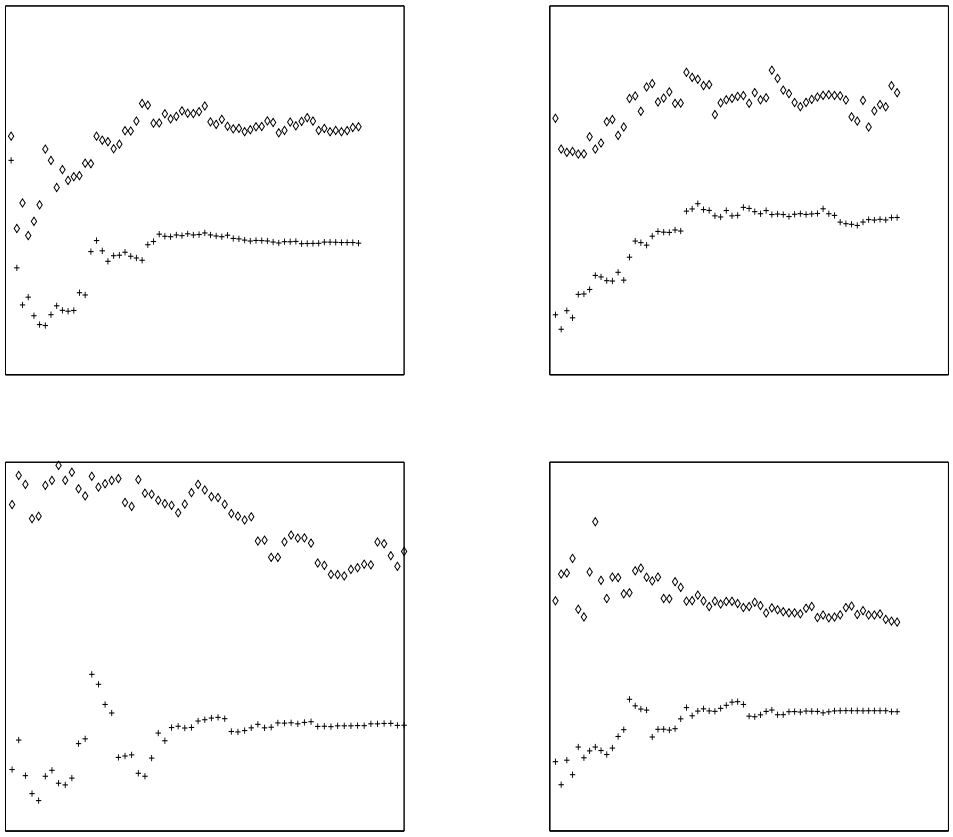

Figure 9: **LSCF** - Frequency estimates as a function of model order (x-axis). Input/output modes are represented by '+'; output-only poles by diamonds. Two different modes are shown (Top - bottom) for data lengths of 10000 (Left) and 20000 (Right).

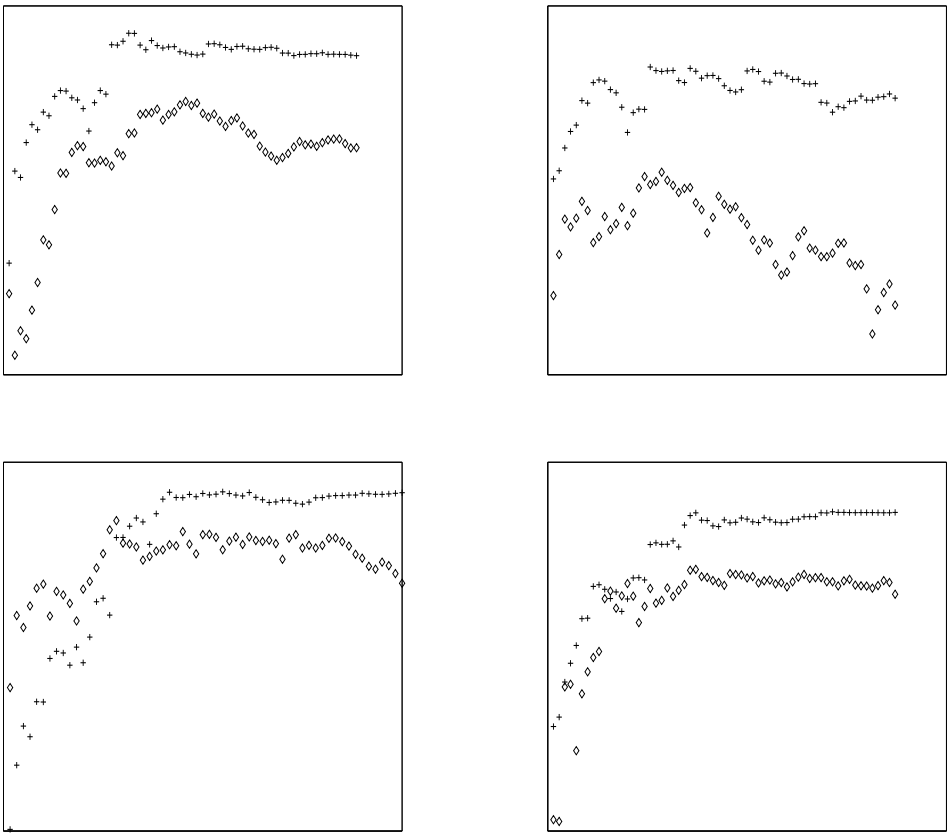

Figure 10: **LSCF** - Damping estimates as a function of model order (x-axis). Input/output modes are represented by '+'; output-only poles by diamonds. Two different modes are shown (Top - bottom) for data lengths of 10000 (Left) and 20000 (Right).

as a function of the model order as displayed on Figures 9 and 10, a positive effect of using the input information is visible: the variation of the output-only poles is larger. From these pictures, it is also clear that the input/output and output-only pole estimates do not coincide. This is probably due to the (slight) coloring of the inputs.

Sample size effect. Changing the sample size is not changing the aspect of the stabilization diagrams dramatically (see Figure 8). From Figures 9 and 10, it can be concluded that the frequency and damping variations as a function of model order slightly decreases when more samples are used.

5 Further comments and conclusions

We have discussed two classes of eigenstructure identification methods, the so-called subspace and polyreference LSCF methods, each of which working either with input/output or output-only data. The covariance-driven subspace identification method has been implemented within two toolboxes: the IN-OP module of the LMS software CADA-X, and the modal analysis module of the free INRIA software Scilab [32, 33]. The polyreference LSCF method has been implemented under the name of PolyMAX within the LMS Test.Lab [29].

We have presented the practical capabilities of both classes of methods for non-stationary aircraft structures. For the subspace-based algorithms, the experimental results show that the input/output method performs better than the output-only one on real data. For long samples, the loss in accuracy becomes neglectible. Hence the additional value of using inputs - when available - holds mainly when data samples are short. For the polyreference LSCF methods, similar conclusions can be drawn.

The lesson from this paper is that, when easily available, input sensor data should be used. Of course, when inputs are not measured, then output-only methods are the only remaining ones, and our study demonstrates that the engineer should not be worried using them. In some cases, whether using or not input measurements can be a design choice: the cost of installing corresponding sensors can be balanced with the slight loss of accuracy than could result.

Acknowledgments

This work has been carried out within the Eureka projects no 1562 SINOPSYS (Model based **S**tructural monitoring using **in-op**eration **sys**tem identification) coordinated

by LMS, Leuven, Belgium, and no 2419 FLITE (**Fli**ght **T**est **E**asy), coordinated by Sopemea, Velizy-Villacoublay, France.

The contribution of Arnaud Guyader to an early version of the subspace-based input/output methods described in section 2, of Yann Veillard to the development of the Scilab toolbox, and of Auguste Sam to the experimental results in section 4.5, are acknowledged.

Appendix: State-space model for structural analysis

The use of state-space representations for modal analysis is well known [16, 22, 35]. For the sake of completeness, we briefly recall the main equations and parameters. We assume that the behavior of the system can be described by a stationary linear dynamical system, and that, in the frequency range of interest, the input forces can be modeled as a non-stationary white noise. Consequently the relevant model is the matrix differential system:

$$\left\{ \begin{array}{rcl} M\ddot{\mathcal{Z}}(t) + C\dot{\mathcal{Z}}(t) + K\mathcal{Z}(t) & = & \nu(t) \\ Y(t) & = & L\mathcal{Z}(t) + \varepsilon(t) \end{array} \right. \tag{34}$$

where t denotes continuous time, M, C, K are the mass, damping and stiffness matrices respectively, (high dimensional) vector $\mathcal{Z}$ collects the displacements of the degrees of freedom of the structure; the external (non measured) force ν is modeled as a non-stationary white noise with time-varying covariance matrix $Q_\nu(t)$, measurements are collected in the (often, low dimensional) vector Y, matrix L states where the sensors are located, and ε is a white measurement noise.

The *modes* or eigenfrequencies-frequencies denoted generically by μ, and the *mode-shapes* or eigenvectors denoted generically by ψ_μ, are solutions of:

$$\det(M\mu^2 + C\mu + K) = 0 \ , \quad (M\mu^2 + C\mu + K)\ \Psi_\mu = 0 \ , \quad \psi_\mu = L\ \Psi_\mu \tag{35}$$

Sampling the model in Eq. (34) at rate $1/\tau$ yields the discrete time model in state space form:

$$\left\{ \begin{array}{rcl} X_k & = & F\ X_{k-1} + W_k \\ Y_k & = & H\ X_{k-1} + v_k \end{array} \right. \tag{36}$$

where the state and the output are:

$$X_k = \left[\begin{array}{c} \mathcal{Z}(k\tau) \\ \dot{\mathcal{Z}}(k\tau) \end{array} \right] \ , \ Y_k = Y(k\tau), \tag{37}$$

the state transition and observation matrices are :

$$F = e^{\mathcal{L}\tau}, \quad \mathcal{L} = \begin{bmatrix} 0 & I \\ -M^{-1}K & -M^{-1}C \end{bmatrix}, \quad H = [L \;\; 0],$$

and where state noise W_k contains both a measured input U_k and an *unmeasured*, Gaussian, zero-mean, white noise V_k, with covariance matrix: $Q_k \stackrel{\Delta}{=} \mathbf{E}\left(V_k\, V_k^T\right)$ where $\mathbf{E}(.)$ denotes the expectation operator. State X and observed output Y have dimensions $n = 2m$ and r respectively, with r (often much) smaller than n in practice. The assumptions on the noises are discussed in section 2.

The eigenstructure (λ, Φ_λ) of the state transition matrix F results from :

$$\det(F - \lambda\, I) = 0\ , \quad F\ \Phi_\lambda = \lambda\ \Phi_\lambda$$

and the modal parameters defined in (35) are then deduced as :

$$e^{\tau\mu} = \lambda, \quad \psi_\mu = \varphi_\lambda \stackrel{\Delta}{=} H\ \Phi_\lambda \tag{38}$$

The collection of pairs $(\lambda, \varphi_\lambda)$ form a canonical parameterization[2] of the pole part of the system in (36), referred to as the system eigenstructure.

References

[1] Abdelghani, M., Chou, C.T., & Verhaegen, M. (1997). Using subspace methods in the identification and modal analysis of structures. *Proceedings of the 15th International Modal Analysis Conference*, Orlando, Florida (pp.1392–1398).

[2] Abdelghani, M., Goursat, M., & Biolchini, T. (1999). On-line monitoring of aircraft structures under unknown excitation. *Mechanical Systems Signal Processing*, 13(6), pp.839–853.

[3] Akaïke, H. (1973). Markovian representation of stochastic processes by canonical variables. *SIAM Journal of Control*, 13, pp.162–173.

[4] Akaïke, H. (1974). Stochastic theory of minimal realization. *IEEE Automatic Control*, 19, pp.667–674.

[5] Arun, K.S., & Kung, S.Y. (1986). Generalized principal components analysis and its application in approximate stochastic realization. In *Modeling and Application of Stochastic Processes*, U.B. Desai, Ed., Kluwer Academic Publishers, pp.75–103.

[2] A parameterization invariant w.r.t. changes in the state basis.

[6] Basseville, M., Abdelghani, M., & Benveniste, A. (2000). Subspace-based fault detection algorithms for vibration monitoring. *Automatica*, 36(1), pp.101–109.

[7] Basseville, M., Benveniste, A., Goursat, M., Hermans, L., Mevel, L., & Van der Auweraer, H. (2001). Output-only subspace-based structural identification: from theory to industrial testing practice. *ASME Journal of Dynamic Systems Measurement and Control*, 123(4), pp.668–676.

[8] Bauer, D. (2003). Choosing integer parameters in subspace methods: a survey on asymptotic results. *Proceedings of the 13th IFAC/IFORS Symposium on Identification and System Parameter Estimation, SYSID'2003*, Rotterdam, NL.

[9] Bauer, D., Deistler, M., & Scherrer, W. (1999). Consistency and asymptotic normality of some subspace algorithms for systems without observed inputs. *Automatica*, 35, pp.1243–1254.

[10] Bauer, D., & Jansson, M. (2000). Analysis of the asymptotic properties of the MOESP type of subspace algorithms. *Automatica*, 36, pp.497–509.

[11] Bauer, D., & Ljung, L. (2002). Some facts about the choice of the weighting matrices in Larimore type of subspace algorithms. *Automatica*, 38, pp.763–773.

[12] Benveniste, A., & Fuchs, J.-J. (1985). Single sample modal identification of a non-stationary stochastic process. *IEEE Automatic Control*, 30(1), pp.66–74.

[13] Caines, P.E. (1988). *Linear Stochastic Systems.* Wiley Series in Probability and Mathematical Statistics.

[14] Cauberghe, B., Guillaume, P., Verboven, P., Parloo, E., & Vanlanduit, S. (2004). A polyreference implementation of the maximum likelihood complex frequency-domain estimator and some industrial applications. *Proceedings of the 22th International Modal Analysis Conference*, Dearborn, Michigan.

[15] Deblauwe, F., Allemang, R.J., & Brown D.L. (1987). The polyreference time domain technique. *Proceedings of the 5th International Modal Analysis Conference* (pp.832–845).

[16] Ewins, D.J. (2000). *Modal Testing: Theory, Practice and Applications* (2nd ed). Research Studies Press, Letchworth, Hertfordshire, UK.

[17] Guillaume, P., Pintelon, R., & Schoukens, J. (1996). Accurate estimation of multivariable frequency response functions. *Proceedings of the 13th IFAC Triennal World Conference*, San Francisco, California (pp.423–428).

[18] Guillaume, P., Verboven, P., Vanlandult, S., Van der Auweraer, H., & Peeters, B. (2003). A polyreference implementation of the least-squares complex frequency domain estimator. *Proceedings of the 21th International Modal Analysis Conference*, Orlando, Florida.

[19] Guyader, A., & Mevel, L. (2003). Covariance-driven subspace methods: input/output vs. output-only. *Proceedings of the 21th International Modal Analysis Conference*, Orlando, Florida.

[20] Hannan, E.J., & Deistler, M. (1988). *The Statistical Theory of Linear Systems.* Wiley Series in Probability and Mathematical Statistics.

[21] Heylen, W., Lammens, S., & Sas, P. (1995). *Modal Analysis Theory and Testing.* Mechanical Engineering Dept, Katholieke Universiteit Leuven, Leuven, B.

[22] Juang, J.N. (1994). *Applied System Identification.* Prentice Hall, NJ.

[23] Kailath, T. (1980). *Linear systems.* Prentice Hall, NJ.

[24] Kehoe, M.W. (1995). A historical overview of flight flutter testing. *NASA Technical Memorandum* **4720**.

[25] Lembregts, F., Snoeys, R., & Leuridan, J. (1987). Application and evaluation of multiple input modal parameter estimation. *Journal of Modal Analysis*, 2(1), pp.19–31.

[26] Lindquist, A., & G. Picci (1996). Canonical correlation analysis, approximate covariance extension, and identification of stationary time series. *Automatica*, 32(5), pp.709–733.

[27] Ljung, L. (1999). *System Identification - Theory for the User (2nd Edition).* PTR Prentice Hall, Upper Saddle River, N.J.

[28] LMS International (2000). *The LMS Theory and Background Book.* Leuven, Belgium, `http://www.lmsintl.com`.

[29] LMS International. (2004). *LMS Test.Lab - Structural Testing Rev 4B.* Leuven, Belgium, `http://www.lmsintl.com`.

[30] Marple, S.L. (1987). *Digital spectral analysis*. Prentice-Hall, New York, USA.

[31] Mevel, L., Benveniste, A., Basseville, M., & Goursat, M. (2002). Blind subspace-based eigenstructure identification under non-stationary excitation using moving sensors. *IEEE Transactions on Signal Processing*, 50(1), pp.41–48.

[32] Mevel, L., Goursat, M., & Benveniste, A. (2003). Using subspace on flight data, a practical example. *Proceedings of the 21th International Modal Analysis Conference*, Orlando, Florida.

[33] Mevel, L., Goursat, M., Basseville, M., & Benveniste, A. (2003). Subspace-based modal identification and monitoring of large structures, a Scilab toolbox. *Proceedings of the 13th IFAC/IFORS Symposium on Identification and System Parameter Estimation, SYSID'2003*, Rotterdam, NL. `http://www.irisa.fr/sigma2/constructif/modal.htm`.

[34] Ottersten, B., Viberg, M., & Kailath, T. (1992). Analysis of subspace fitting and ML techniques for parameter estimation. *IEEE Transactions on Signal Processing*, 40, pp.590–599.

[35] Peeters, B., & De Roeck, G. (1999). Reference-based stochastic subspace identification for output-only modal analysis. *Mechanical Systems and Signal Processing*, 13(6), pp.855–878.

[36] Peeters, B., Guillaume, P., Van der Auweraer, H., Cauberghe, B., Verboven, P., & Leuridan, J. (2004). Automotive and aerospace applications of the PolyMAX modal parameter estimation method. *Proceedings of the 22th International Modal Analysis Conference*, Dearborn, Michigan.

[37] Pickrel, C.R., & White, P.J. (2003). Flight flutter testing of transport aircraft: in-flight modal analysis. *Proceedings of the 21st International Modal Analysis Conference*, Kissimmee, Florida.

[38] Pintelon, R., & Schoukens, J. (2001). *System Identification: a Frequency Domain Approach*. IEEE Press, New York, USA.

[39] Prevosto, M., Olagnon, M., Benveniste, A., Basseville, M., & LeVey, G. (1991). State-space formulation, a solution to modal parameter estimation. *Journal Sound and Vibration*, 148, pp.329–342.

[40] De Roeck, G., Peeters, B., & Ren, W.-X. (2000). Benchmark study on system identification through ambient vibration measurements. *Proceedings of the 18th International Modal Analysis Conference*, San Antonio, Texas (pp.1106–1112).

[41] Soderström, T., & Stoïca, P. (1989). *System Identification*. Prentice Hall.

[42] Van der Auweraer, H. (2003). System identification for structural dynamics and vibroacoustics design engineering. Plenary lecture, *Proceedings of the 13th IFAC/IFORS Symposium on Identification and System Parameter Estimation, SYSID'2003*, Rotterdam, NL.

[43] Van Overschee, P., & De Moor, B. (1996). *Subspace Identification for Linear Systems: Theory, Implementation, Applications*. Kluwer Academic Publishers.

[44] Van Overschee, P., & De Moor, B. (1994). N4SID: Subspace algorithms for the identification of combined deterministic-stochastic systems. *Automatica*, 30(1), pp.75–93.

[45] Viberg, M. (1995). Subspace-based methods for the identification of linear time-invariant systems. *Automatica*, 31(12), pp.1835–1853.

[46] Viberg, M., Wahlberg, B., & Ottersten, B. (1997). Analysis of state space system identification methods based on instrumental variables and subspace fitting. *Automatica*, 33(9), pp.1603–1616.

Contents

1 Introduction **3**

2 Subspace-based eigenstructure identification **5**
2.1 Fundamentals of covariance-driven identification algorithms 5
2.2 Handling time domain input/output data 6

3 Polyreference LSCF or PEM for eigenstructure identification **10**
3.1 The input/output polyreference LSCF method 10
3.2 The output-only polyreference LSCF method 13

4 Experimental results **13**
4.1 Practical implementation issues - Subspace algorithms 14
4.2 Practical implementation issues - Polyreference LSCF algorithms . . 16
4.3 Practical implementation issues - Stabilization diagrams 16
4.4 Industrial testing requirements 16
4.5 Real application example 18
4.5.1 Results with the subspace-based algorithms 18
4.5.2 Results with the polyreference LSCF algorithms 22

5 Further comments and conclusions **27**

Acknowledgments **27**

Appendix: State-space model for structural analysis **28**

References **29**

Unité de recherche INRIA Lorraine, Technopôle de Nancy-Brabois, Campus scientifique,
615 rue du Jardin Botanique, BP 101, 54600 VILLERS LÈS NANCY
Unité de recherche INRIA Rennes, Irisa, Campus universitaire de Beaulieu, 35042 RENNES Cedex
Unité de recherche INRIA Rhône-Alpes, 655, avenue de l'Europe, 38330 MONTBONNOT ST MARTIN
Unité de recherche INRIA Rocquencourt, Domaine de Voluceau, Rocquencourt, BP 105, 78153 LE CHESNAY Cedex
Unité de recherche INRIA Sophia-Antipolis, 2004 route des Lucioles, BP 93, 06902 SOPHIA-ANTIPOLIS Cedex

Éditeur
INRIA, Domaine de Voluceau, Rocquencourt, BP 105, 78153 LE CHESNAY Cedex (France)
http://www.inria.fr
ISSN 0249-6399